Journal of Polymers and the Environment (2021) 29:1576–1590
https://doi.org/10.1007/s10924-020-01977-4

ORIGINAL PAPER

Preparation of Novel Magnetic Sodium Alginate-Ferric(III) Gel Beads and Their Super-Efficient Removal of Direct Dyes from Water

Ting Lv[1,2] · Beigang Li[1,2]

Accepted: 16 November 2020 / Published online: 25 November 2020

Abstract

Novel magnetic sodium alginate-based biopolymer Fe_3O_4@SA-Fe was successfully prepared by the cross-linking reaction of sodium alginate (SA) and Fe(III) ions and adding magnetic ferric oxide (Fe_3O_4), and characterized by Scanning Electron Microscopy (SEM), Energy Dispersive Spectroscopy (EDS), UV-visible diffuse reflectance spectroscopy (UV-Vis DRS), Fourier Transform-Infrared (FTIR), X-ray Photoelectron Spectroscopy (XPS) and Vibrating Sample Magnetometer (VSM), respectively. The effects of preparation and adsorption conditions on the adsorbent were investigated by adsorbing Congo red (CR) and Direct red 23 (DR 23) dyes. The results showed that the synthesized Fe_3O_4@SA-Fe polymer gel beads exhibited super-high adsorption property and good stability when the mass concentrations of SA, Fe(III) ions and Fe_3O_4 are 16, 12.5 and 7 g/L at room temperature respectively. The adsorption rates of two dyes by Fe_3O_4@SA-Fe were very fast at 298 K, and the time required to reach the equilibrium was very short, which was 30 min for CR and 60 min for DR 23. Moreover, the dye removal efficiencies were over 99.4% and 95.2% in a wide pH range of 2.0 ~ 9.0 for CR and 2.0 ~ 10.0 for DR 23, respectively. The adsorption process could be accurately described by the pseudo-second-order rate model, which were mostly controlled by intra-particle diffusion. The fitting results of isothermic data by Langmuir, Freundlich and Dubinin-Radushkevich (D-R) models revealed that the equilibrium data completely obeyed the Langmuir model and the obtained maximum adsorption capacities of CR and DR 23 were 3333 and 1429 mg/g at 298 K, respectively. FTIR, UV-Vis and XPS analysis indicated that the electrostatic adsorption, hydrogen bonding and ligand exchange promoted the interaction between dye molecules and Fe_3O_4@SA-Fe. A green magnetic biosorbent Fe_3O_4@SA-Fe gel beads with simple preparation method and high-cost performance can be used for super-efficient purification of high-concentration dye effluent and quickly separated from the aqueous phase and recovered, which would have a good application prospect.

Keywords Sodium alginate · Magnetism · Ferric iron · Biopolymer · Dye adsorption

Introduction

Over the years, a large amount of dye wastewater has been produced due to the wide application of various dyes in food, textile printing and dyeing, leather, paper, plastic and other fields [1]. Without treatment or incomplete treatment, the colored dye wastewater discharged into the environmental water body can bring serious water environmental pollution and harm to human health. In particular, azo dyes are one of the most widely used synthetic dyes, accounting for more than half of the total dyes. Under special conditions, azo dyes can decompose to produce a variety of carcinogenic aromatic amines, which may cause human diseases and cancer after activation [2–7]. Therefore, azo-dye wastewater must be treated innocuously before discharge. As two frequently-used water-soluble anionic dyes, direct dyes congo red (CR) and direct red 23 (DR 23) are azo dyes used widely due to their molecular linear structure and the good coplanarity of aromatic ring structure. Therefore, efficient treatment methods must be selected for the purification of this kind of wastewater. Among the common water treatment technologies, including various physical, chemical and biological methods [8–10], the research and application of adsorption technology has been paid wide attention

✉ Beigang Li
libeigang_1964@126.com

[1] Chemistry & Environment Science College, Inner Mongolia Normal University, Hohhot 010022, People's Republic of China

[2] Inner Mongolia Key Laboratory of Environmental Chemistry, Hohhot 010022, People's Republic of China

due to its convenient operation, high efficiency of wastewater treatment and low energy consumption. Especially in recent years, more and more attraction has been focused on the development of natural biomaterials such as alginate, chitosan and cellulose as adsorbents for the removal of heavy metals and organic pollutants from various industrial wastewater [11–14]. These biological materials have been widely used as the matrix to prepare various environmental-friendly adsorption materials with better adsorption properties by chemical reaction or composite action with other materials [15–17]. However, there are still some problems in the application of adsorbents, such as the high cost of adsorbent, the difficulty of separating powder adsorbents from aqueous phase after adsorbing pollutants and the risk of secondary pollution. Accordingly, the traditional adsorbents can be made into macroparticles and magnetized by adding magnetic Fe_3O_4 particles to realize rapid separation and recovery by the action of external magnetic field after adsorption, which will make them have better practical application value [18–22]. A novel magnetic/activated charcoal/β-cyclodextrin/alginate (Fe_3O_4/AC/CD/Alg) polymer nanocomposite was prepared and used to adsorb cationic dye. The experimental results indicated that the removal efficiency and adsorption capacity of methylene blue onto Fe_3O_4/AC/CD/Alg were 99.53% and 10.63 mg/g in 90 min, respectively [23]. Ge et al. [24] used magadiite–magnetite (MAG-Fe_3O_4) nanocomposite for removal of methylene blue from aqueous solutions and the adsorption capacity and removal efficiency of methylene blue onto MAG-Fe_3O_4 were 93.7 mg/g and 96.2%, respectively. The magnetic zeolite-alginate-polyanetholesulfonic acid gel beads (m-ALG/PESA) were applied to cationic dyes adsorption and the maximum adsorption capacities of methylene blue and malachite green onto m-ALG/PESA gel beads were 400 mg/g and 164 mg/g, respectively [25].

Sodium alginate (SA) is a copolymer composed of consecutive sequence of GM、MM and GG blocks formed by β-D-1,4-mannanic acid (M-unit) and α-L-1,4-guluronic acid (G-unit) through the link of 1,4-glycosidic bond. There are abundant carboxyl and hydroxyl groups in the molecular chains of SA. As a natural polysaccharide, SA has many advantages, such as strong hydrophilicity, biosafety, biodegradability, non-toxic side effects, low cost and rich sources, so it is widely used in food industry, pharmaceutical industry and other industries [26–29]. The occurrence of ionic crosslinking reaction by replacing sodium ions with polyvalent metal ions can make SA form the gel spheres with three-dimensional structure [30], which will turn into an ideal matrix for the preparation of SA-based composite materials with stronger adsorption performance and better separation property [31–33].

In the current study, novel magnetic alginate-Fe(III) polymer gel spheres were prepared by selecting Fe(III) ions as crosslinking ions and adding magnetic Fe_3O_4 particles, and used for the ultra-efficient removal of CR and DR 23 dyes from aqueous solutions. The related research has not been reported. The important conditions of preparation and adsorption affecting the properties of magnetic composite were investigated. The adsorption efficiency and magnetic separation performance of the magnetic polymer were evaluated, and the adsorption mechanism was discussed by adsorption study and material characterization. It would be expected to obtain a green and pollution-free magnetic biopolymer adsorbent with low-cost performance and ultra-high adsorption capacity for direct dyes, and achieve rapid separation and recovery of the magnetic gel beads from aqueous phase after adsorption.

Materials and Methods

Materials and Reagents

SA, Fe_3O_4 and ferric chloride hexahydrate ($FeCl_3{\cdot}6H_2O$) were purchased respectively from Tianjin Damao Chemical Reagent Factory, Institute of Guangfu Fine Chemicals and Windboat Chemical Reagent Technology Co., Ltd., China, which are of analytical pure grade. CR and DR 23 dyes with the wavelength corresponding to absorption maximum (λ_{max}) of 498 nm and 502 nm were purchased from Shanghai Jiaying Chemical Co., Ltd., China. The chemical structures of CR (molecular formula $C_{32}H_{22}N_6Na_2O_6S_2$, relative molar mass 696.68 g/mol) and DR 23 ($C_{35}H_{25}N_7Na_2O_{10}S_2$, relative molar mass 790.69 g/mol) are shown in Fig. 1.

Preparation and Characterization of Magnetic Polymer Fe_3O_4@SA-Fe Gel Beads

0.40 g SA was dissolved in deionized water with magnetic stirring for 1 h at 298 K to obtain the uniformly dispersed solution, then 0.175 g Fe_3O_4 was added into SA solution and further stirred and ultrasonically dispersed to a uniform mixed solution. The mixed solution was slowly dropped into 12.5 g/L $FeCl_3$ solution with slow stirring and the gel beads were continuously generated. After 4 h of crosslinking polymerization, the brown black gel beads were removed, washed with deionized water to neutral and dried. The magnetic biosorbent Fe_3O_4@SA-Fe was successfully synthesized.

The surface morphology and elemental distribution of SA, SA-Fe and Fe_3O_4@SA-Fe polymer gel beads were characterized by scanning electron microscopy and energy dispersive spectroscopy (SEM-EDS, S-4800, Hitachi, Japan). The functional structures of materials were analyzed by a Nicolet Nexus 6700-type Fourier transform infrared spectrometer (FTIR,

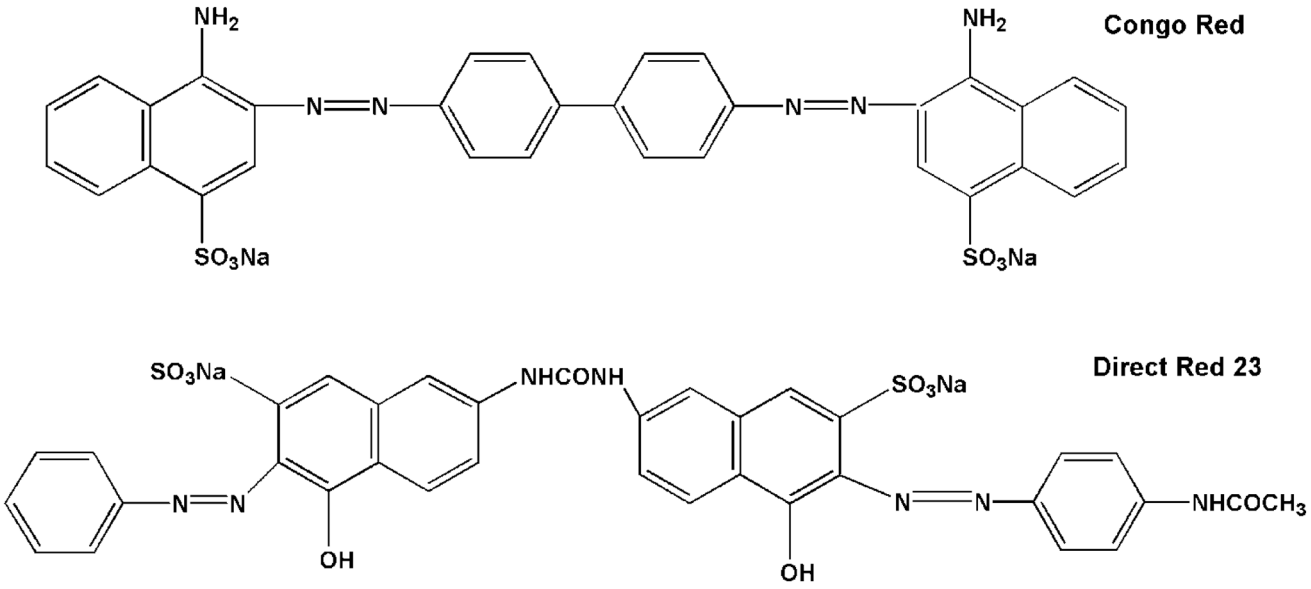

Fig. 1 The chemical structures of CR and DR 23

KBr tableting method, Thermo Fisher Scientific Inc., U.S.A) and U-2900 ultraviolet visible diffuse reflection spectrometer (UV-Vis DRS, $BaSO_4$ tableting method, Hitachi Inc., Japan). The elemental status was studied by an Axis Ultra type X-ray Photoelectron Spectroscopy (XPS, Shimadzu Inc., Japan). The magnetic hysteresis loops of samples were determined by JDAW-2000D type vibrating sample magnetometer (VSM, Yingpu Magnetoelectric Technology Development Co., Ltd., China) at room temperature.

Adsorption Experiment

The adsorbent Fe_3O_4@SA-Fe with fixed mass (0.030 g for CR, 0.025 g for DR 23) was added to a series of conical flasks containing certain-concentration dye solutions and shaken for 2 h in a water bath thermostatic oscillator at 298 K. The mixture was then filtered through 0.45 μm microfiltration membrane and the dye concentration in each filtrate was measured by means of spectrophotometry at λ_{max} of each dye. The equilibrium adsorption capacity q_e (mg/g) and removal rate η (%) of dyes were calculated by use of the following equations.

$$q_e = \frac{(C_0 - C_e)V}{m} \quad (1)$$

$$\eta = \frac{(C_0 - C_e)}{C_0} \times 100\% \quad (2)$$

where C_0 (mg/L) and C_e (mg/L) are the concentrations of the dye solutions before and after the adsorption, respectively, V (L) is the dye solution volume, m (g) is the adsorbent mass.

Results and Discussion

Preparation Conditions of Fe_3O_4@SA-Fe Polymer

The adsorption properties of SA-based polymer hydrogel depend strongly on the choice of SA solution concentration during preparation, which determines the pelletizing property, mechanical properties and stability of gel beads. Accordingly, the effect of SA solution concentration on the polymer properties was discussed. As shown in Fig. 2a, when the concentration of SA solution increased from 14 to 17.2 g/L, the removal efficiencies of two dyes by Fe_3O_4@SA-Fe were only slightly reduced from 99.6 to 92.8% for CR and from 99.7 to 97.8% for DR 23, and then decreased significantly with the increase of SA concentration at 298 K. It was found simultaneously that when the concentration of SA solution was lower than 14 g/L, the spheroidization of magnetic polymer was poor, however, when the SA concentration was higher than 18 g/L, it was difficult to produce uniform crosslinking polymerization because of the high viscosity of SA solution. Therefore, a 16 g/L concentration of SA solution was chosen to prepare composite gel beads.

Fe(III) ions as a crosslinking agent is the key factor to make SA hydrogel polymerized into spheres. It can be clearly seen from Fig. 2b that the adsorption capacities and removal efficiencies of two dyes onto prepared Fe_3O_4@SA-Fe polymer increase significantly with the increase of Fe(III) ion concentration from 5 to 12.5 g/L, and then remain basically unchanged as the Fe(III) ion concentration continues to increase from 12.5 to 30 g/L. This indicates that the 12.5 g/L of Fe(III) concentration can synthesize the magnetic gel beads with the best adsorption

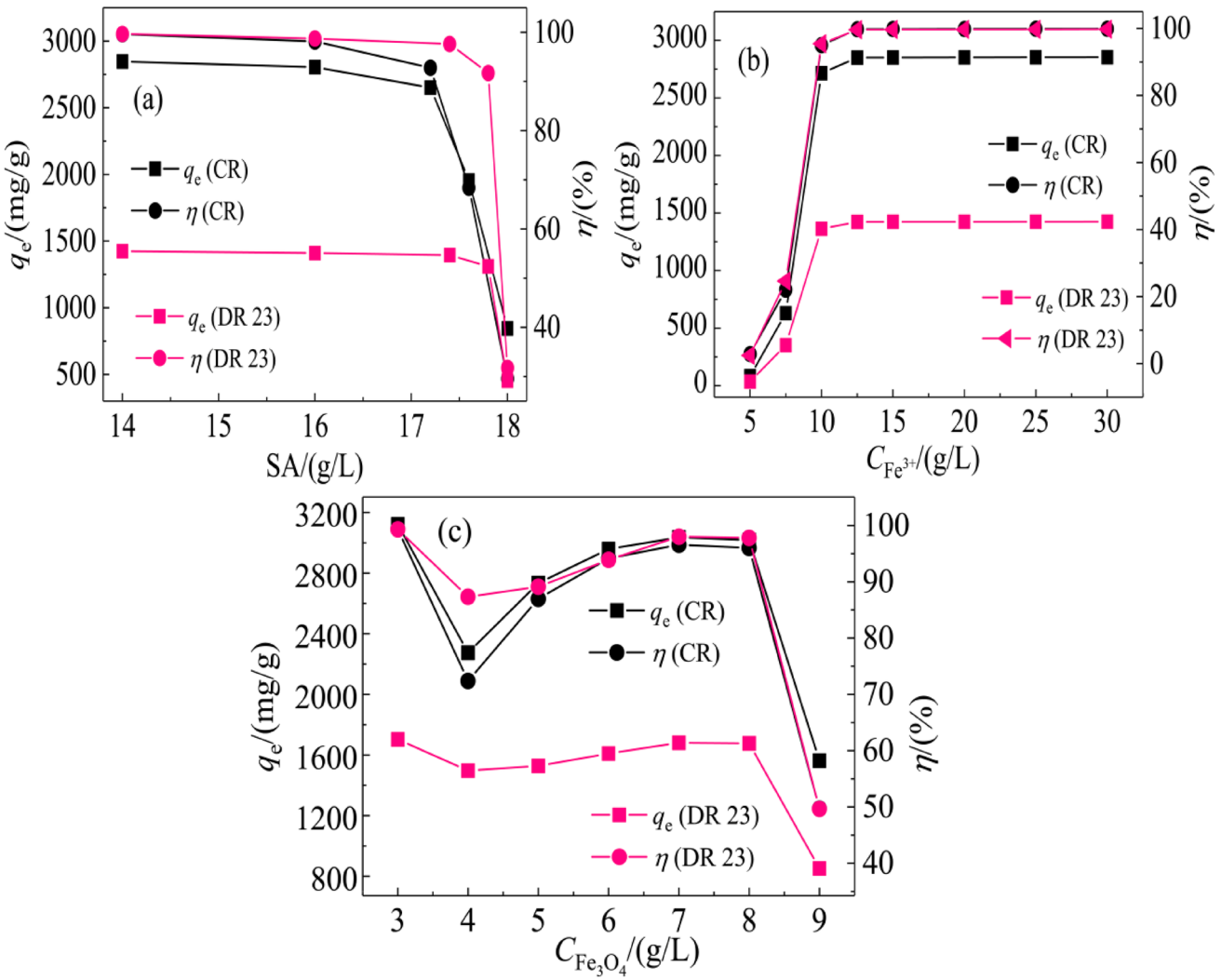

Fig. 2 Effect of the mass concentration of SA (**a**), Fe^{3+} (**b**) and Fe_3O_4 (**c**)

property through perfect crosslinking with SA, so it is selected for the preparation of magnetic polymer.

The purpose of adding Fe_3O_4 in polymer gel beads is to make the polymer adsorbent has magnetism to realize the rapid separation of solid and liquid phases through the external magnetic field, and also change the adsorbent performance at the same time. The concentrations of SA and Fe(III) ion solutions were fixed at 16 and 12.5 g/L respectively, the effect of Fe_3O_4 concentration on the properties of synthesized magnetic polymer is given in Fig. 2c. Although the prepared Fe_3O_4@SA-Fe had the best adsorption effect for two dyes when the concentration of Fe_3O_4 was 3 g/L, its magnetic property was too weak to realize magnetic separation. Hence, considering comprehensively, the choice of 7 g/L Fe_3O_4 concentration was most suitable for the preparation of magnetic polymer Fe_3O_4@SA-Fe with better performance.

The surface morphology of SA and polymer Fe_3O_4@SA-Fe gel beads was characterized through SEM. It is displayed in Fig. 3a that SA primarily consists of massive and schistose fragment in various ways. The brown black Fe_3O_4@SA-Fe polymer beads obtained by crosslinking SA with Fe(III) ions and Fe_3O_4 are shown in Fig. 3b, c. Each gel bead with a diameter of about 1.36 mm emerges a "cauliflower like" surface which is composed entirely of seemingly ordered grooves and wrinkles. This surface structure is very conducive to the adsorption of pollutants. Meanwhile, there are scattered white spots on the bead surface, which may be the magnetic Fe_3O_4 particles in Fig. 3d. After further EDS analysis, it was found from Table 1 that the higher contents of Fe and Cl elements were found in the polymer, but not in SA. The Na content in the polymer decreased significantly compared with that in SA. These changes further confirmed that the exchange reaction between Fe(III) ions and Na^+ ions

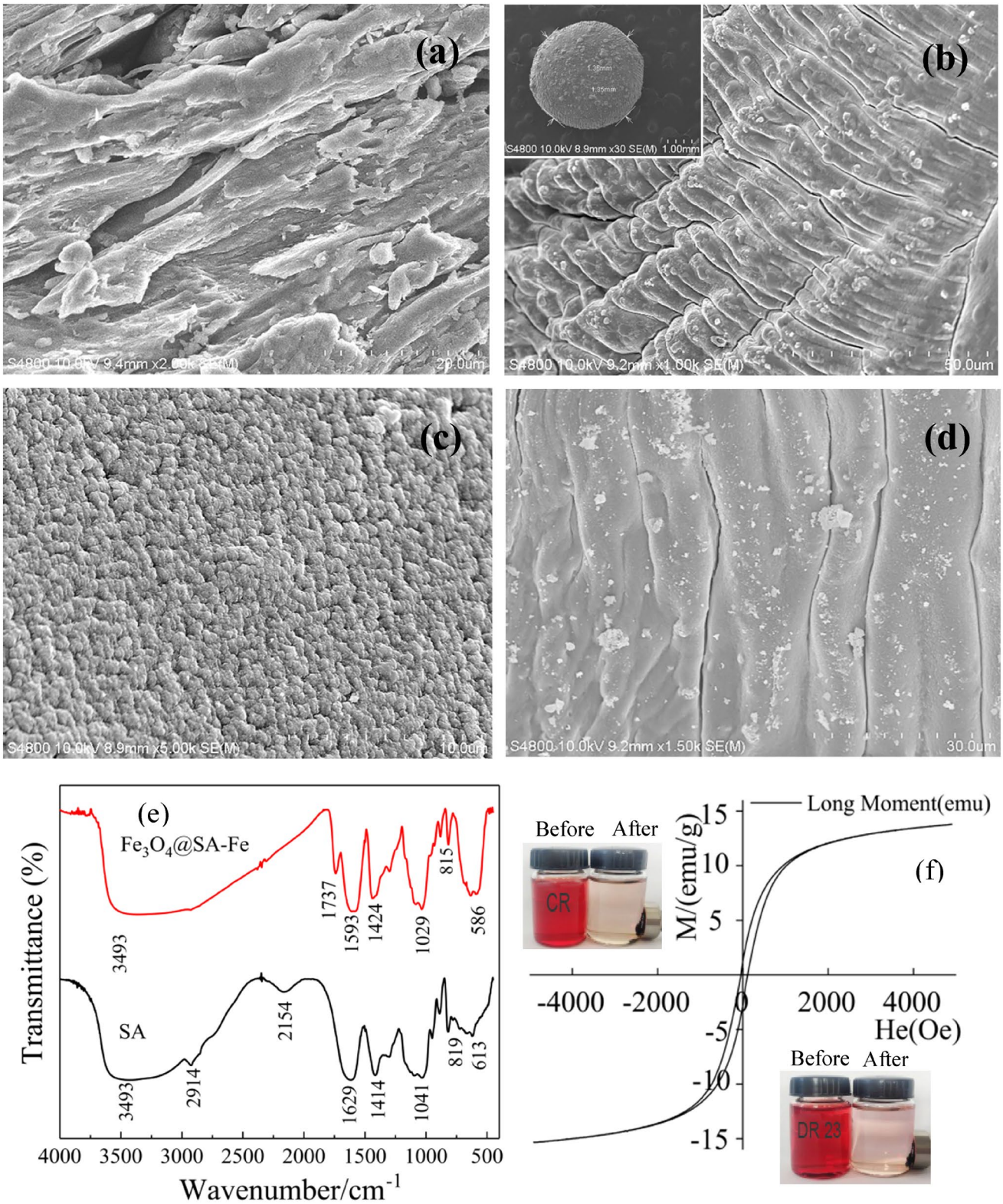

Fig. 3 SEM images of SA (**a**), SA-Fe (**b**, **c**), Fe_3O_4@SA-Fe polymer gel beads (**d**), FTIR (**e**), and magnetic hysteresis loop (**f**) analysis

Table 1 The EDS analysis of SA and Fe_3O_4@SA-Fe polymer gel beads

Sample	Element content / (%)				
	C	O	Na	Fe	Cl
SA	35.6	54.6	9.8	0	0
Fe_3O_4@SA-Fe	14.46	22.0	0.7	32.3	20.5

in SA molecules occurred, and continued to crosslink with SA chains to form magnetic Fe_3O_4@SA-Fe polymer gel beads with three-dimensional structure.

FTIR spectra of SA and Fe_3O_4@SA-Fe polymer are presented in Fig. 3e. The broad peak for SA at 3284 ~ 3612 cm^{-1} emanates from stronger intermolecular hydrogen bonding [34]. The other absorption bands at 2914, 1629, 1414 and 1041 cm^{-1} should be attributed to the stretching vibration of C-H, asymmetric and symmetric stretching vibrations of $-COO^-$ and the stretching vibration of C-O-C, respectively [35]. In the spectrum of Fe_3O_4@SA-Fe polymer, the three peaks of $-COO^-$ and C-O-C groups in the spectrum of SA were shifted to 1593, 1424 and 1029 cm^{-1}, respectively, illustrating that the occurrence of crosslinking polymerization between Fe(III) ions and $-COO^-$ and C-O-C groups in SA molecules. Meanwhile, the new peak appeared at around 586 cm^{-1} should be assigned to the Fe-O bond, suggesting that Fe_3O_4 was also involved in polymerization.

The measured saturation magnetization value of Fe_3O_4@SA-Fe was 13.79 emu/g (Fig. 3f). In the presence of an external magnetic field near the bottle wall, the magnetic polymer gel beads after adsorption of two dyes can be quickly gathered onto the bottle wall, indicating that the magnetic properties of the polymer gel beads can achieve the separation of the adsorbent quickly and effectively from the treated wastewater, which would be very important for the recovery of adsorbent and the avoidance of the secondary pollution in practical application. Meanwhile, the coercivity of Fe_3O_4@SA-Fe was 101.5 Oe, which can be used as a permanent magnetic material [36].

Effect of Important Adsorption Factors

When the dosage of Fe_3O_4@SA-Fe adsorbent was 0.030 and 0.025 g for CR and DR 23 adsorption respectively, the change of dye adsorption capacity and removal rate with the initial concentrations of dyes was shown in Fig. 4a. The adsorption capacity increased first and then decreased with the increase of initial concentration of each dye, while the removal efficiencies reached the maximum values with 99.8% and 99.4% for CR and DR 23 at 2000 mg/L and 1000 mg/L concentrations respectively, and then decreased gradually with the increase of dye concentration. This was because there were enough active sites on the polymer surface to adsorb a number of dye molecules, but the dye-adsorbed amount per the unit mass adsorbent could only decrease with increasing dye concentration when the adsorption sites were saturated.

The solution pH is a key parameter affecting the adsorption owing to the changes of the charge on the adsorbent surface and the existing forms of dyes with the solution acidity. The influence of solution pH value on the CR and DR 23 adsorption by Fe_3O_4@SA-Fe composite was studied in the range of pH 2.0 ~ 11.0 as shown in Fig. 4b. The adsorption capacities and removal efficiencies of CR and DR 23 onto Fe_3O_4@SA-Fe at pH 2.0 reached the maximum values with 3166 mg/g, 1395 mg/g, 100% and 99.6%, respectively, and then almost unchanged with pH increase from 2.0 to 9.0, and finally reduced rapidly with the further increase of pH. Similar results have also been reported in literature [17, 37]. However, the removal rate of DR 23 could still reach 95.2% at pH 10.0. The electrostatic interaction between the adsorbent surface with positive charge via protonation and dye anions increased with the decrease of pH in acidic solution, leading to the significant increase of adsorption capacities. Under alkaline conditions, the electrostatic repulsion between dye anions and adsorbent by deprotonation should be enhanced with the increase of pH, resulting in the decrease of adsorption capacities. But in fact, the adsorption capacity and removal efficiency for two dyes did not change significantly under the alkaline conditions of pH ≤ 9.0 (pH ≤ 10.0 for DR 23), suggesting that there should be other adsorption mechanisms, such as hydrogen bonding or chemical adsorption except electrostatic adsorption. The rich -OH, -COOH and $-SO_3^-$ groups on Fe_3O_4@SA-Fe surface readily formed hydrogen bonds with direct dye molecules containing $-NH_2$, -OH, -N=N- groups and phenyl. Therefore, the natural acidity of each dye solution (pH 8.0 for CR solution and pH 9.0 for DR 23 solution respectively) was selected to perform the following adsorption study, which was more convenient for practical operation. The results show that the Fe_3O_4@SA-Fe polymer with ultra-high adsorption capacity, nearly 100% dye removal efficiency and wide pH application range has greater advantages than the adsorption materials reported in references [38, 39], and can realize the rapid separation and recovery from liquid phase.

The effect of contact time and temperature on dye adsorption by Fe_3O_4@SA-Fe is presented in Fig. 4c. The adsorption rates of CR and DR 23 were exceedingly fast and the basic adsorption equilibrium can be reached in 20 min at 298 K, and the corresponding adsorption capacities prominently rose to 2442 mg/g and 929 mg/g, respectively, which was very beneficial to the practical application of dye wastewater treatment because of the reduction of investment cost and the significant improvement of treatment efficiency. In addition, it was found from Fig. 4c that the adsorption rates

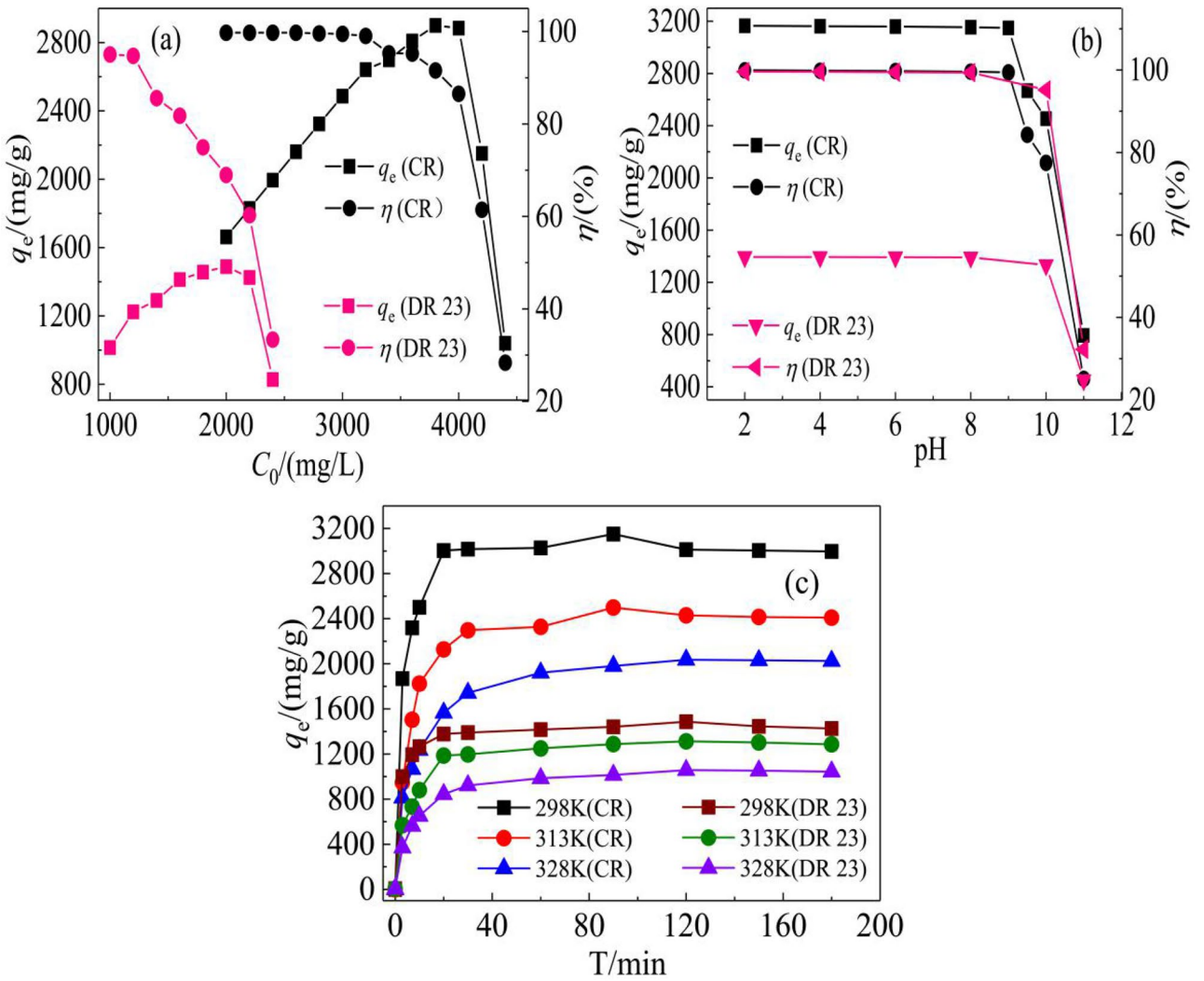

Fig. 4 Effect of dye concentration (**a**), pH (**b**), contact time and temperature (**c**) on adsorption

of two dyes onto Fe_3O_4@SA-Fe gel beads decreased with the rise of temperature from 298 K to 328 K, but the dynamic adsorption equilibrium could still be reached within 30 min, proving that the two adsorption reactions were all of exothermic nature and the room temperature would be more conducive to the operation of the adsorption system.

Adsorption Kinetics

Pseudo-first-order, pseudo-second-order and intraparticular diffusion models were used to fit all kinetic experimental data at different temperatures (298, 313 and 328 K) to investigate mechanism of adsorption process and rate determining step. The concrete expressions of three models are as follows [40, 41]:

$$\lg\left(q_e - q_t\right) = \lg q_e - \frac{k_1}{2.303}t \tag{3}$$

$$\frac{t}{q_t} = \frac{1}{k_2 q_e^2} + \frac{1}{q_e}t \tag{4}$$

$$q_t = k_p t^{1/2} + I \tag{5}$$

where k_1 (min^{-1}), k_2 [g/(mg·min)] and k_p ($mg/g{\cdot}min^{1/2}$) are the first-order, second-order and intraparticular diffusion rate constants, respectively; q_t and q_e (mg/g) are the amount of dye adsorbed at time t (min) and equilibrium, correspondingly.

The fitting parameters and correlation coefficient (R^2) obtained by kinetic models and the error analysis (sum of squared error, SSE; root mean squared error, RMSE)

by using origin software [42] are listed in Table 2. The R^2 values ($R^2 > 0.999$) fitted by the pseudo-second-order rate model were nearly 1.000 at different temperatures, which were significantly better than those obtained by the pseudo-first-order model ($R^2 > 0.362$). The values of SSE and RMSE calculated for the pseudo-second-order model fitting were remarkably lower than those for pseudo-first-order model fitting. Meanwhile, the values of $q_{e,2}$ calculated by the pseudo-second-order model approached the values of actual equilibrium adsorption capacities (q_{exp}), confirming that the whole adsorption process of CR and DR 23 onto Fe_3O_4@SA-Fe polymer can be formulated by the pseudo-second-order rate model. In addition, the k_2 values of two dye sorption decrease with increasing temperature, demonstrating the exothermic nature of adsorption reaction.

The fitting results of the experimental data by the intraparticle diffusion model at different temperatures are presented in Fig. 5a, b and Table 2, respectively. The occurrence of dye adsorption processes could be considered as two aspects. The adsorption data of first rapid stages from 3 to 20 min for CR and from 3 to 10 min for DR 23 had good goodness-of-fit for the intraparticle diffusion model based on the values of correlation coefficient (R^2), illustrating that the adsorption rate of the process was mainly controlled by intraparticle diffusion. The last stages were basically in the dynamic adsorption equilibrium processes of two dyes (the upper platforms of the curves), which were also affected by the intraparticle diffusion, but not the only rate-limiting step.

Adsorption Isotherms

The adsorption isotherms drawn from the equilibrium data obtained by isothermal experiments at different temperatures are presented in Fig. 5c, d. The adsorption capacity of each dye onto Fe_3O_4@SA-Fe polymer decreased with the increase of temperature from 298 K to 328 K. Three isotherm models known as the Langmuir, Freundlich and Dubinin-Radushkevich (D-R) models were used to discuss the adsorption behavior of dyes on the magnetic polymer adsorbent, and expressed as follows [43, 44], respectively:

Langmuir:

$$\frac{C_e}{q_e} = \frac{C_e}{q_{max}} + \frac{1}{q_{max} b} \tag{7}$$

Freundlich:

$$\log q_e = \frac{\log_{C_e}}{n} + \log k_F \tag{8}$$

Dubinin-Radushkevich:

$$\ln q_e = \ln q_{max} + \beta\varepsilon^2 \tag{9}$$

$$\varepsilon = RT \ \ln(1 + 1/C_e) \tag{10}$$

$$E = 1/\sqrt{-2\beta} \tag{11}$$

where q_{max} (mg/g) represents the the maximum adsorption capacity; b (L/mg) is the Langmuir adsorption coefficient; k_F and n are Freundlich constants related to adsorption; β (mol^2/J^2) is the constant associated with adsorption energy; ε and E (kJ/mol) are the Polanyi potential and the mean energy of adsorption. In addition, the separation factor R_L given by Langmuir, which is equal to $1/(1 + bc_0)$, was applied to illustrate the difficult and easy nature of adsorption [45, 46].

The important parameters and error analysis obtained by fitting the equilibrium data of CR and DR 23 sorption onto Fe_3O_4@SA-Fe using three isothermal models at various temperatures are listed in Table 3. Based on the comparison of the analytical results in Table 3, the linear fitting of Langmuir model gave the highest R^2 values ($R^2 \geq 0.999$) and the lower values of SSE and RMSE, and the maximum adsorption capacities (q_{max}) of CR and DR 23 were 3333 mg/g and 1429 mg/g at room temperature (298 K), respectively. The Langmuir adsorption coefficients (b) decreased with the increase of temperature. The values of q_{max} for two dyes on Fe_3O_4@SA-Fe were also close to the experimental values ($q_{e,exp}$) at three temperatures (298 K ~ 328 K). These revealed that the Langmuir model was most suitable to explain the dye adsorption behavior with a monomolecular layer and the exothermic nature of the adsorption systems, which were consistent with the kinetic results. This confirmed that the room temperature would be the most favorable for the ultra-efficient removal of CR and DR 23 dyes and also very convenient for the actual operation of dye wastewater treatment. Compared with the reported literature values of maximum adsorption capacity (q_{max}) of CR and DR 23 onto other different types of adsorbents [29, 47–61] in Table 4, the magnetic polymer Fe_3O_4@SA-Fe revealed a greater advantage because it has greater adsorption capacities for two dyes, and could quickly recover from the aqueous phase after adsorption and did not produce secondary pollution. Hence, polymer Fe_3O_4@SA-Fe gel beads may be considered a promising green adsorbent for super-efficient removal of direct dyes. In addition, the values of separation factor R_L with the range of 0.0028 ~ 0.0319 in Fig. 5e suggested the easy adsorption reaction for two dyes on Fe_3O_4@SA-Fe.

Meanwhile, the equilibrium data were in good agreement with D-R model ($R^2 \geq 0.903$), and the values of the obtained mean energy (E, kJ/mol) of adsorption were in the range of 19.3 ~ 27.7 kJ/mol for CR and 22.7 ~ 24.1 kJ/mol for DR 23

Table 2 Kinetic fitting relevant parameters of two dyes adsorption on Fe_3O_4@SA-Fe polymer gel beads

	Dye name	CR			DR 23		
	T (K)	298	313	328	298	313	328
	q_{exp} (mg/g)	3150	2499	1981	1396	1232	991
Pseudo-first-order	k_1 (min^{-1})	0.01	0.02	0.05	0.02	0.02	0.03
	$q_{e,1}$ (mg/g)	322	501	840	192	325	404
	R^2	0.3622	0.7496	0.9955	0.6086	0.7692	0.8801
	SSE	0.8533	0.4944	0.0052	0.4408	0.7943	0.4596
	RMSE	0.1219	0.0706	0.0013	0.0630	0.1135	0.0657
Pseudo-second-order	k_2 [g/(mg·min^{-1})]	0.0005	0.0002	0.0001	0.0007	0.0003	0.0002
	$q_{e,2}$ (mg/g)	3333	2500	2000	1429	1250	1000
	R^2	0.9994	0.9992	0.9990	0.9995	0.9992	0.9990
	SSE	2.83×10^{-6}	5.76×10^{-6}	9.11×10^{-6}	1.17×10^{-5}	2.07×10^{-5}	4.02×10^{-5}
	RMSE	3.15×10^{-7}	6.40×10^{-7}	1.01×10^{-6}	1.30×10^{-6}	2.30×10^{-6}	4.46×10^{-6}

	T/min		CR			T/min	DR 23		
			298	313	328		298	313	328
Intraparticle diffusion	3-20 min	*Kp* (mg/g·$min^{1/2}$)	409	426	276	3-10 min	178	202	187
		I	1193	321	342		634	173	23.3
		R^2	0.9920	0.9355	0.9968		0.9887	0.9855	0.9973
	After 30 min	*Kp* (mg/g·$min^{1/2}$)	Dynamic equilibrium			20-60 min	11.4	19.0	30.4
		I					1242	1025	632
		R^2					0.9995	0.9772	0.9249

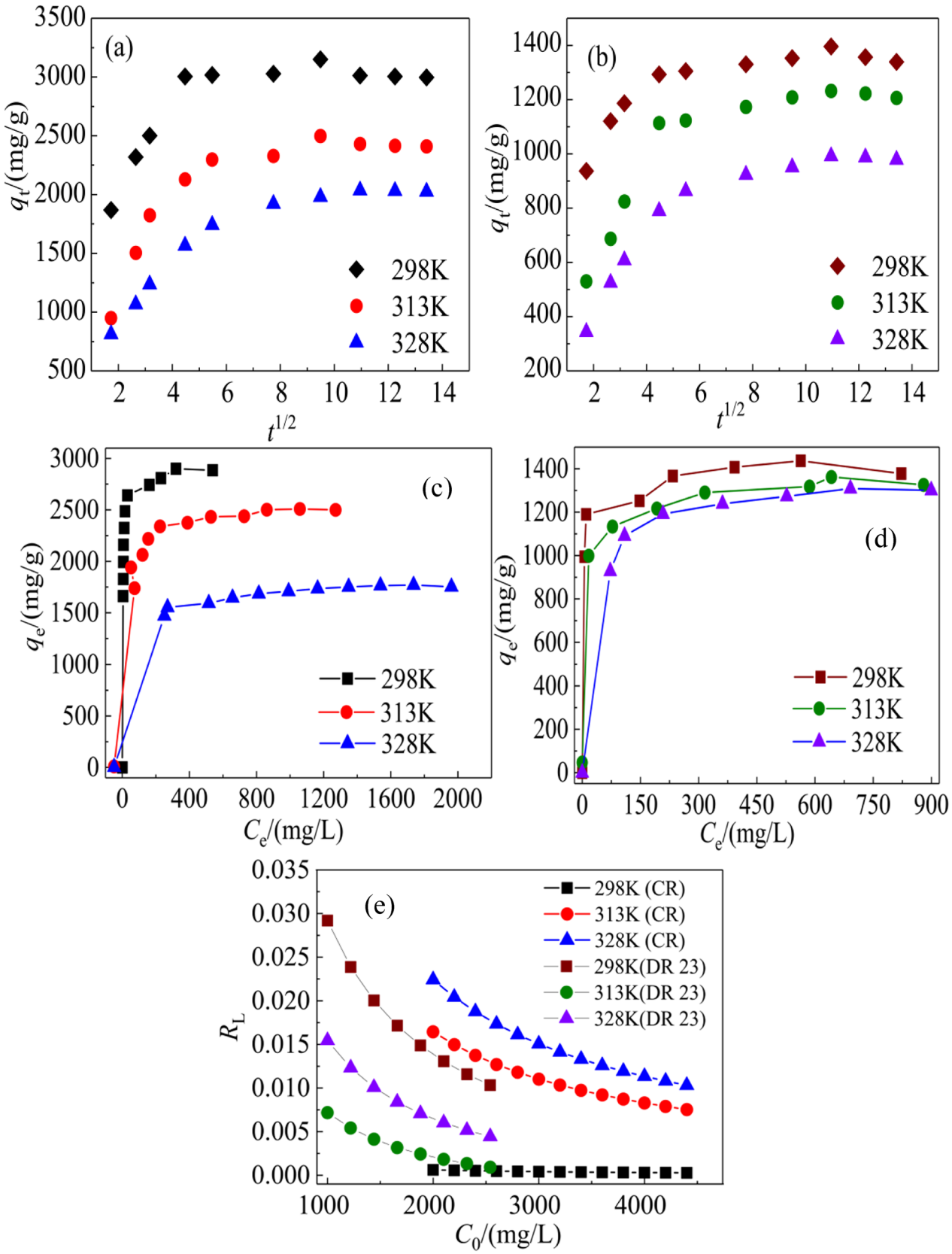

Fig. 5 Fitting curves of intraparticle diffusion for CR (**a**) and DR 23 (**b**), isotherms adsorption of CR (**c**) and DR 23 (**d**), and the plot of R_L versus C_0 (**e**)

Table 3 Isothermal fitting parameters of Langmuir and Freundlich models at different temperatures

	Dye name	CR			DR 23		
	T (K)	298	313	328	298	313	328
Langmuir models	q_{max} (mg/g)	3333	2500	1667	1429	1429	1250
	b (L/mg)	0.3000	0.0299	0.0218	0.3043	0.0946	0.0531
	R^2	0.9994	0.9990	0.9989	0.9990	0.9992	0.9990
	SSE	1.37×10^{-5}	3.62×10^{-4}	0.0014	3.38×10^{-4}	3.49×10^{-4}	3.93×10^{-4}
	RMSE	1.37×10^{-6}	3.62×10^{-5}	1.43×10^{-4}	5.63×10^{-5}	5.82×10^{-5}	6.55×10^{-5}
Freundlich models	n	10.7	8.39	11.2	16.5	12.3	8.19
	K_F	1708	1006	880	957	788	591
	R^2	0.7800	0.8018	0.9370	0.8514	0.9734	0.8772
	SSE	0.0154	0.0055	4.39×10^{-4}	0.0029	3.98×10^{-4}	0.0021
	RMSE	0.0017	6.14×10^{-4}	4.88×10^{-5}	5.69×10^{-4}	7.96×10^{-5}	4.28×10^{-4}
Dubinin-Radushkevich (D-R) models	q_{max} (mg/g)	3270	2550	2033	1637	1517	1530
	β (mol^2/kJ^2)	−0.00065	−0.00086	−0.0013	−0.00086	−0.00085	−0.00097
	E (kJ/mol)	27.7	24.1	19.3	24.1	24.2	22.7
	R^2	0.9157	0.9341	0.9782	0.9739	0.9878	0.9938
	SSE	0.0067	8.37×10^{-4}	2.10×10^{-4}	0.0024	6.49×10^{-4}	5.75×10^{-4}
	RMSE	0.0011	1.40×10^{-4}	3.50×10^{-5}	7.90×10^{-4}	3.24×10^{-4}	1.15×10^{-4}

in Table 3, indicating the occurrence of chemical adsorption and hydrogen bonding between the adsorbent and dye molecules [62].

In addition, the adsorption results showed that the adsorption capacity of CR by Fe_3O_4@SA-Fe was significantly higher than that of DR 23. This should be mainly because the relative molar mass of DR 23 (790.69 g/mol) is much larger than that of CR (696.68 g/mol) and the molecular chains of DR 23 are markedly longer than those of CR, which will lead to a smaller number of molecules adsorbed on the unit surface area of adsorbent, so its adsorption capacity will be relatively lower.

Discussion on Adsorption Mechanism

The UV-Vis spectra of Fe_3O_4@SA-Fe before and after adsorption of two dyes were displayed in Fig. 6a. The wavelength corresponding to absorption maximum of the adsorbent at $\lambda_{max}=407$ nm were moved to 412 nm, 415 nm and 478 nm after CR and DR 23 adsorption, respectively, and the two absorption bands became wider. These changes confirmed the interaction between the adsorbent and each dye molecules.

In the FTIR spectrum of Fe_3O_4@SA-Fe polymer (Fig. 6b), the changes of different characteristic peaks after dye adsorption are as follows: the asymmetric and symmetric stretching vibrations of -COO^- groups were shifted from 1593 and 1424 cm^{-1} to 1622 and 1416 cm^{-1} for Fe_3O_4@SA-Fe-CR and 1616 cm^{-1} and 1413 cm^{-1} for Fe_3O_4@SA-Fe-DR 23, respectively. The absorption peaks of C-O-C were moved from 1029 to 1046 cm^{-1} and 1036 cm^{-1} for CR and DR 23 adsorption, respectively. The peak of Fe-O bond has changed concurrently from 586 cm^{-1} to 616 cm^{-1} and 612 cm^{-1}, respectively. In addition, the intensity of these peaks also varied more or less. These changes confirmed the chemical and hydrogen bond interreaction between Fe_3O_4@SA-Fe polymer gel beads and dye molecules [63], and Fe_3O_4 particles in Fe_3O_4@SA-Fe polymer also participated in the interaction with dye anions.

In order to further study the interaction between the adsorbent and dye molecules, the surface chemistry of the adsorbent before and after adsorption were analyzed by XPS as shown in Fig. 7. The XPS wide scan spectra of Fe_3O_4@SA-Fe polymer in Fig. 7a clearly showed the presence of characteristic peaks such as C 1 s, O 1 s, and Fe 2p, confirming that these elements are the main components of Fe_3O_4@SA-Fe polymer. However, after dye adsorption, the adsorbent spectrum changed slightly in the position and intensity of energy band of the main elements. It is found from the high-resolution C 1 s spectra of Fe_3O_4@SA-Fe before and after dye adsorption in Fig. 7b that C 1 s spectrum of Fe_3O_4@SA-Fe can be decomposed into three peaks with binding energy at 284.8, 286.6, and 288.8 eV, respectively,

Table 4 Comparison of the maximum adsorption of CR and DR 23 onto various adsorbents

Dye name	Adsorbents	Maximum adsorption capacity (mg/g)	Reference
CR	WS	41.2	[47]
	Na-MMT	58.2	[48]
	CMC-MMT	81.8	
	pMWCNT/β-CD/TiO2-Ag nanosponge polyurethane composite	147.0	[49]
	Gum Ghatii -Acrylamide grafted copolymer coated with Zero valent Iron	153.3	[50]
	DOX KCF-100	240	[51]
	CR KCF-100	547	
	NCPPY	299.0	[52]
	C/NF	448.4	[53]
	PSI-PA	522.2	[54]
	Y /SA hydrogel	1567	[37]
	Fe_3O_4@SA-Fe polymer gel beads	3333	This study
DR 23	Cationized sawdust	65.8	[55]
	rGO/CTAB	79.0	[56]
	CS-g-PNEANI	112	[57]
	montmorillonite nanoclay	166.6	[58]
	modified nanofibe	370	[59]
	AS-CTAB	454.9	[60]
	FPAN2	1250	[61]
	Fe_3O_4@SA-Fe polymer gel beads	1429	This study

which should be attributed to the C atom in C – C, C – O, and COO^- [64], respectively. After dye adsorption, the binding energy of each peak can be shifted slightly and the area ratio of each peak can be reduced. The two peaks of O1s spectrum for Fe_3O_4@SA-Fe (Fig. 7c) at 530.6 and 532.6 eV assigned to the O atom in iron-oxide (Fe-O) and COO^- [65] were shifted to 530.3 and 532.7 eV for CR and 530.3 and 532.3 eV for DR 23 after dye adsorption, respectively, and the area ratio of each peak at 530.6 and 532.6 eV can be increased. The area ratios of peak corresponded to O spectrum of Fe-O and COO^- are 1:3 and 1:2 for Fe_3O_4@SA-Fe and Fe_3O_4@SA-Fe-CR and 1:1.6 and 1:1.4 for Fe_3O_4@SA-Fe and Fe_3O_4@SA-Fe-DR 23, respectively. In the high-resolution spectrum of Fe 2p in Fig. 7d, the spectra of Fe $2p_{3/2}$ and Fe$2p_{1/2}$ for Fe_3O_4@SA-Fe were respectively divided into two peaks at 711.1 eV and 712.9 eV, 723.8 eV and 725.8 eV [66], indicating the existence of Fe^{3+} and Fe^{2+} and the existence of Fe_3O_4 component in the adsorbent [67]. Among them, the peaks at 711.1 eV and 723.8 eV could be assigned to Fe^{2+} and the peaks at 712.9 eV and 725.8 eV could be attributed to Fe^{3+} [68, 69]. After dye adsorption, each peak of the Fe species for Fe_3O_4@SA-Fe was moved. Before and after CR adsorption, the area ratios of Fe^{2+} peaks for Fe_3O_4@SA-Fe are 1:1.5 and 1:3, and those of Fe^{3+} peaks are 1:1.4 and 1:3 in Fig. 7e, respectively. After DR 23 adsorption, the peak areas of Fe^{2+} peaks can increase by 1:1.4 and 1:1.8 times, respectively, and the areas of Fe^{3+} peaks for Fe_3O_4@SA-Fe can increase by 1:1.4 and 1:2 times as shown in Fig. 7f, respectively. These changes of XPS spectra confirmed that the carboxyl groups of SA and Fe-O groups in iron-oxide were involved in dye adsorption through hydrogen bonding between carboxyl and hydroxyl

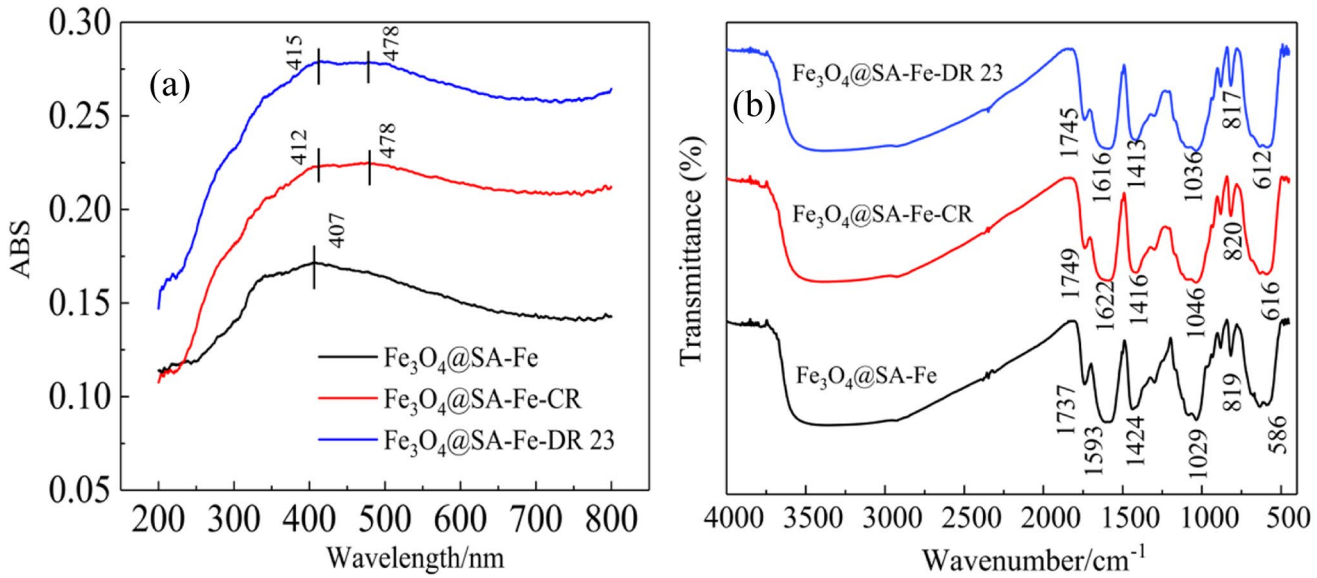

Fig. 6 UV-Vis DRS (**a**) and FTIR (**b**) spectra of Fe_3O_4@SA-Fe before and after adsorption of two dyes

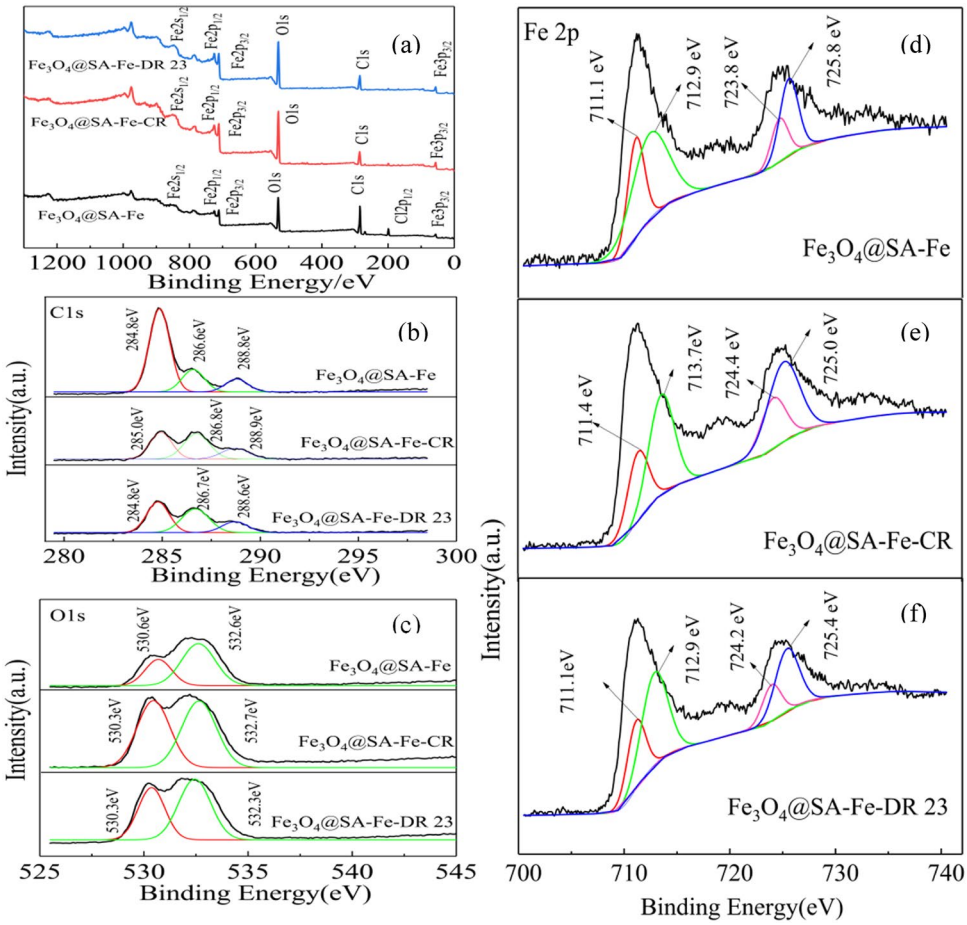

Fig. 7 Full survey XPS spectrum (**a**) of Fe_3O_4@SA-Fe polymer gel beads before and after two dyes adsorption: high-resolution C1s (**b**), O1s (**c**) and Fe2p (**d**, **e**, **f**)

groups of Fe_3O_4@SA-Fe and dye molecules and surface complexation (Fe-O-dye), which agreed well with the results of UV-Vis and FTIR analysis.

According to the effect of pH on the adsorbent performance and the results of UV-Vis, FTIR and XPS characterization and adsorption study, it can be deduced that the adsorption of dye anions onto Fe_3O_4@SA-Fe gel beads is chiefly related to electrostatic adsorption, hydrogen bonding and surface complexation besides Van der Waals forces (Fig. 8).

Conclusion

Magnetic polymer Fe_3O_4@SA-Fe gel beads synthesized by facile droplet polymerization at room temperature exhibiting super-high adsorption efficacy for CR and DR 23 dyes in a wide pH range of dyeing wastewater. The optimized ratio of raw materials for polymer gel beads preparation was obtained. The adsorption of two dyes onto Fe_3O_4@SA-Fe gel beads can reach equilibrium very quickly, which was 30 min for CR and 60 min for DR 23, respectively. The adsorption processes at different temperatures can be completely represented by the pseudo-second-order rate model and basically controlled by the intraparticle diffusion. Based on the best goodness-of-fit of equilibrium data for the Langmuir model and the exothermic properties of adsorption systems, the maximum adsorption capacities of two dyes can reach 3333 and 1429 mg/g at 298 K and natural pH of dye solutions respectively, significantly better than those of many other reported adsorbents. Analysis of FTIR, UV-Vis and XPS and the discovery of adsorption study suggested that the interaction mechanism between Fe_3O_4@SA-Fe adsorbent and dye molecules involved primarily electrostatic adsorption, hydrogen bonding and chemical complexation. As a feasible and cost-effective magnetic polymer, Fe_3O_4@SA-Fe gel beads with wide application range of acidity, the best adsorption effect and the most convenient practical operation at room temperature and short adsorption equilibrium time, would be considered as a promising environment-friendly biosorbent, which can achieve the ultra-efficient purification for high-concentration dye effluent and fast separation and recovery from treated-water.

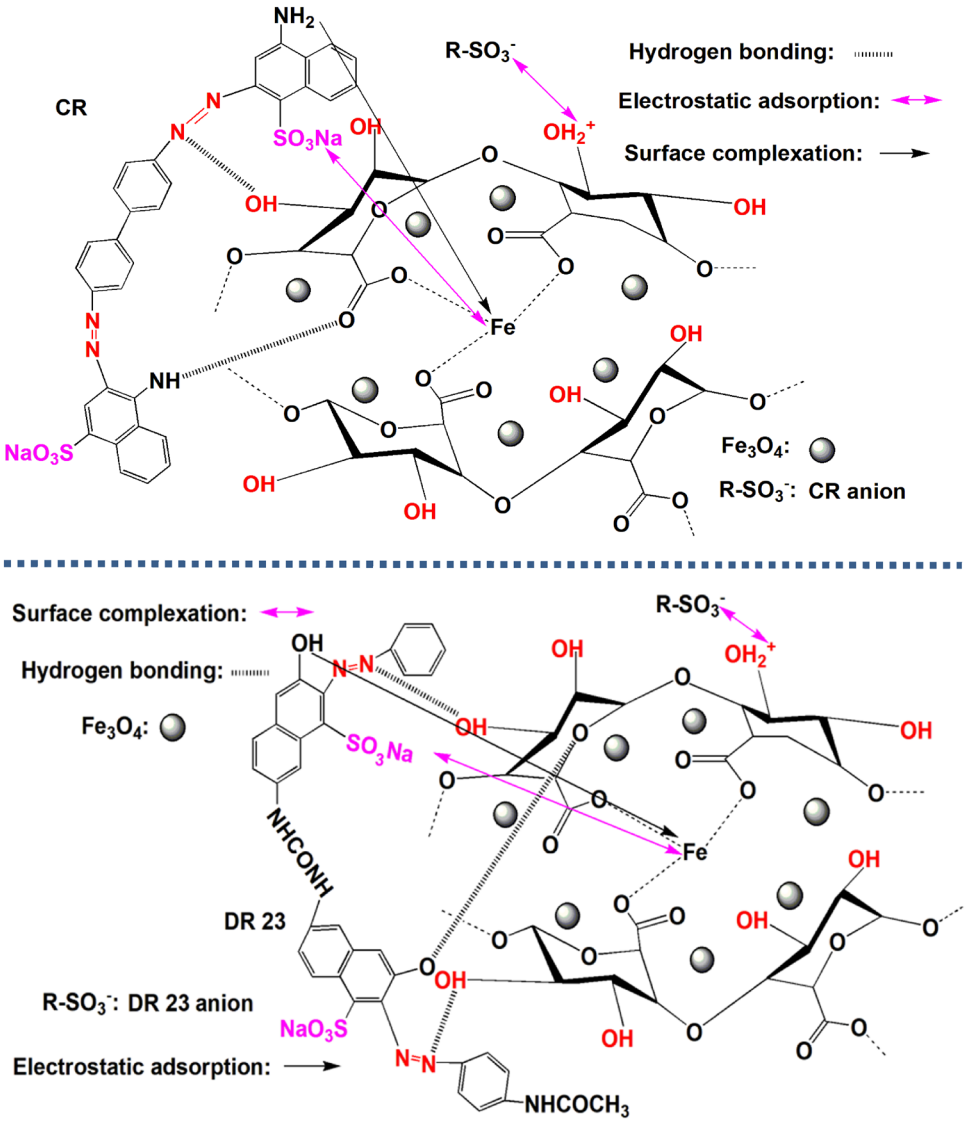

Fig. 8 Diagrammatic sketch of CR and DR 23 dyes anion adsorption onto Fe_3O_4@SA-Fe

Acknowledgments This study was supported by the National Natural Science Foundation of China (21167011), the Natural Science Foundation of Inner Mongolia Autonomous Region (2020LH02009), the Science Research Foundation of Inner Mongolia Normal University (112129K18ZZYF006) and Research and Innovation Foundation for Postgraduates of Inner Mongolia Normal University (CXJJS19119).

References

1. Zhuang HF, Tang HJ, Shan SD, Mao ZR (2019) Ind Water Treat 39:41
2. Li Q, Wang M, Yuan XJ, Li DY, Xu HM, Sun L, P F, X DS (2019) Environ Technol 1
3. Solís M, Solís A, Pérez HI, Manjarrez N, Flores M (2012) Process Biochem 47:1723
4. Deepak R, Vandana M, Radhey Shyam S (2016) Chemosphere 155:591
5. Niu S, Xie XK, Wang Z, Zheng LH, Gao F, Miao Y (2019) Environ Technol :1
6. Yin HX, T YC, H XH, X LP, X MT, H W, W T (2017) Res Environ Sci 30:1105
7. Sun GF, Zeng HY, Song LX, Hu Y, Zhang YQ (2011) J Leshan Normal Univ 26:20
8. Tahreen A, Jami MS, Ali F (2020) J Water Process Eng 37:101440
9. Wang YX, Jiang L, Shang HG, Li Q, Zhou WZ (2020) Environ Technol Innovation 19:1
10. Mishra S, Nayak JKand Maiti A (2020) Clean Technol Envir 22:651
11. Periyasamy S, Naushad M, Viswanathan N (2020) Environ Sci Water Res Technol 6:851
12. Jawad AH, Mubarak NSA, Abdulhameed AS (2020) J Polym Environ 28:624
13. Ren JP, Tao FR, Cui YZ (2020) J Polym Environ 8:1302
14. Yu C, Zhang Y, Fang Y, Tan YJ, Dai K, Liu S, Huang QY (2020) Environ Sci Pollut R 27:16745
15. Ferrer-Polonio E, Fernández-Navarro J, Iborra-Clar M, Alcaina-Miranda M, Mendoza-Roca JA (2020) J Environ Manag 263:110368

16. Yu SY, Cui JL, Wang JB, Zhong CS, Wang X, Wang N (2020) Int J Biol Macromol 149:562
17. Li B, Ren Z (2020) J Polym Environ 28:1811
18. Wang HP, Lin YC, Li Y, Anudari D, Fang H, Guo L, Huang J, Yang JX (2019) J Inorg Organomet Polym Mater 29:1874
19. Rocher V, Siaugue J-M, Cabuil V, Bee A (2008) Water Res 42:1290
20. Elwakeel KZ, El-Bindary AA, El-Sonbati AZ, Hawas AR (2017) Can J Chem 95:807
21. Polat G, Acikel YS (2019) J Polym Environ 27:1971
22. Bée A, Talbot D, Abramson S, Dupuis V (2011) J Colloid Interface 362:486
23. Yadav S, Asthana A, Chakraborty R, Jain B, Singh AK, Carabineiro SAC, Susan MABH (2020) Nanomaterials 10:170
24. Ge M, Xi Z, Zhu C, Liang G, Hu G, Jamal L, Jahangir Alam SM (2019) Polymers 11:607
25. Metin AU, Dogan D, Can M (2020) Mater Chem Phys 256:1
26. Yao WH, Yu F, Ma J (2018) Prog Chem 30:1722
27. Dodero A, Alloisio M, Vicini S, Castellano M (2020) Carbohydr Polym 227:115
28. Zhang M, Bai B, Hu N, Wang HL, So YR (2019) Chem Eng 47:42
29. Zhang J, Lin HQ, Ma QY, Lu BH, Jiang H, Peng BX (2019) China Pharm 30:3307
30. Wang QQ, Liu Y, Zhang CJ, Zhang C, Zhu P (2019) Mater Sci Eng C 99:1469
31. Li ZM, Yao Y, Wei GT, Zhang LY, Lu MJ, Liu L, Liang DX, Sun YQ (2018) J Guangxi Univ (Nat Sci Ed) 43:2391
32. Sun JZ, Wang JX, Ni MJ, Zhang XB, Chen YH, Liu SY, Li H (2019) Environ Sci Technol 42:104
33. Chen WP, Zhang EH, Lin YB (2010) Environ Protection Sci 36:14
34. Verma A, Thakur S, Mamba G, Prateek Gupta RK, Thakur P, Thakur VK (2020) Int J Biol Macromol 148:1130
35. Zhang MY, Yi K, Zhang XW, Han P, Liu W, Tong MP (2020) J Hazard Mater 388:121
36. Li ZQ, Shen JF, Ma HW, Liu X, Shi M, Li N, Ye MX (2012) Polym Bull 68:1153
37. Li BG, Yin HY (2020) J Polym Environ 28:2137
38. Kaur S, Rani S, Mahajan RK (2013) J Chem 2013:1
39. Reza Sohrabi M, Mansouriieh N, Khosravi M, Zolghadr M (2015) Water Sci Technol 71:1367
40. Ho YS, McKay G (1999) Process Biochem 34:451
41. McKay G, Ho YS (1999) Water Res 33:578
42. Anitha T, Senthil Kumar P, Senthil Kumar K (2016) J Water Process Eng 13:127
43. Agnihotri S, Singhal R (2019) J Polym Environ 27:372
44. Tharaneedhar V, Senthil Kumar P, Saravanan A, Ravikumar C, Jaikumar V (2017) Sustain Mater Technol 11:1
45. Foo KY, Hameed BH (2010) Chem Eng J 156:2
46. Kang S, Park S, Park J, Baek K (2019) J Environ Manag 234:181
47. Fawzy MA, Gomaa M (2020) J Environ Manag 262:110380
48. Zhang HL, Ma JZ, Wang FY, Chu YT, Yang L, Xia MZ (2020) Int J Biol Macromol 149:1161
49. Leudjo T, Fosso-Kankeu A, Pillay K, Yangkou Mbianda X (2020) J Environ Chem Eng 8:1
50. Goddeti SMR, Bhaumik M, Maity A, Ray SS (2020) Int J Biol Macromol 149:21
51. Olusegun SJ, Mohallem NDS (2020) Environ Pollut 260:114019
52. Shahnaz T, Mohamed Madhar Fazil S, Paadmanaban VC, Narayanasamy S (2020) Int J Biol Macromol 151:322
53. Hu HJ, Wageh S, Al-Ghamdi AA, Yang SB, Tian ZF, Cheng B, Ho W (2020) Appl Surf Sci 511:1
54. Mansha M, Waheed A, Ahmad T, Kazi IW, Ullah N (2020) Environ Res 184:109337
55. Hebeish A, Ramadan MA, Abdel-Halim E, Abo-Okeil A (2011) Clean Techn Environ Policy 13:713
56. Mahmoodi NM, Maroofi SM, Mazarji M, Nabi-Bidhendi G (2017) J Surfactant Deterg 20:1085
57. Abbasian M, Jaymand M, Niroomand P, Farnoudian-Habibi A, Karaj-Abad SG (2017) Int J Biol Macromolecules 95:393
58. Dalvand A, Mahvi AH (2019) Water Quality Res J 1
59. Mahmoodi NM, Mokhtari-Shourijeh Z, Ghane-Karade A (2017) Water Sci Technol 75:2475
60. Kasperiski FM, Lima EC, Reis GS, Da Costa JB, Dotto GL, Dias SLP (2018) Chem Eng Commun 205:1520
61. Almasian A, Chizari Fard G, Parvinzadeh Gashti M, Mirjalili M, Mokhtari Shourijeh Z (2015) Desalin Water Treat 57:10333
62. Wen RT, Tu BY, Guo XH, Hao XQ, Wu X, Tao HS (2020) Int J Biol Macromol 146:692
63. Mansha M, Waheed A, Ahmad T, Kazi IW, Ullah N (2020) Environ Res 184:109
64. Dong X, Lin YC, Ma YY, Zhao L (2020) Inorg Chim Acta 510:119748
65. Wu ZG, Deng WJ, Zhou W, Luo JW (2019) Carbohyd Polym 216:119
66. Liu Y, Chen JS, Liu ZK, Xu HY, Shi ZQ, Yang QL, Hu GH, Xiong CX (2020) J Colloid Interf Sci 576:119
67. Yamashita T, Hayes P (2008) Applied Surf Sci 254:2441
68. Lu FF, Xu CB, Meng FC, Xia T, Wang RH, Wang JP (2017) Adv Mater Interfaces 4:1700639
69. Lu ZY, Xu WW, Zhu W, Yang Q, Lei XD, Liu JF, Li YP, Sun XM, Duan X (2014) Chem Commun 50:6479